

New Measurement of the Electron Magnetic Moment and the Fine Structure Constant

G. Gabrielse and D. Hanneke

Department of Physics, Harvard University, Cambridge, MA 02138

Abstract. A new measurement resolves the cyclotron and spin levels for a single-electron quantum cyclotron to obtain a dimensionless electron magnetic moment, g , to 7.6 parts in 10^{13} (nearly six times better than in the past) and shifted by 1.7 standard deviations. The new g , with a quantum electrodynamics (QED) calculation, determines the fine structure constant with a 0.7 ppb uncertainty – ten times smaller than for atom-recoil determinations. Remarkably, this 100 mK measurement probes for internal electron structure at 130 GeV.

Keywords: electron magnetic moment, electron g value, fine structure constant, quantum cyclotron
PACS: 13.40.Em, 14.60.Cd, 12.20-m

1. INTRODUCTION

Two of the most fundamental constants of nature are measured much more accurately than ever before – the dimensionless form of the electron magnetic moment [1] and the fine structure constant [2]. The new methods required to achieve such big improvements, developed over 20 years, are summarized here.

Kleppner’s introductory lecture to ICAP reminds us that such precise and fundamental measurements are a central and celebrated tradition of ICAP. This report is offered in the hope that the tradition and diversity of ICAP will continue to include such measurements – because of the important science, and as a fermionic antidote to any bosonic tendency that might make ICAP research condense into too few states.

2. NEW MEASUREMENT OF THE ELECTRON g

Measurements of the electron magnetic moment (μ) probe for internal electron structure and probe the electron’s interaction with the fluctuating vacuum of QED. As an eigenstate of spin \mathbf{S} , the electron (charge $-e$ and mass m) has $\mu \propto \mathbf{S}$,

$$\mu = -g \frac{e\hbar}{2m} \frac{\mathbf{S}}{\hbar}. \quad (1)$$

The g value is a dimensionless measure of the moment, with the dimensions and approximate size given by the Bohr magneton, $e\hbar/(2m)$. If the electron was a mechanical system with an orbital angular momentum, then g would depend upon the relative distributions of the rotating charge and mass, with $g = 1$ for identical distributions. (Cyclotron motion of a charge in a magnetic field B , at frequency $\nu_c = eB/(2\pi m)$, is one example.) A Dirac point particle has $g = 2$. QED predicts that vacuum fluctuations and polariza-

tion slightly increase this value. Electron substructure [3] would make g deviate from the Dirac/QED prediction (as quark-gluon substructure does for a proton).

Measurements of the electron g have a long history [4, 5], with a celebrated measurement [6] providing the accepted value [7] since 1987. Our new g is slightly shifted with a six time smaller uncertainty (Fig. 1a). A one-electron quantum cyclotron [8], cavity-inhibited spontaneous emission [9], a self-excited oscillator (SEO) [10], and a cylindrical Penning trap [11] contribute to the extremely high precision. For the first time, the lowest cyclotron and spin levels of a single electron are fully resolved via quantum non-demolition (QND) measurements [8], and a cavity shift of g is directly observed.

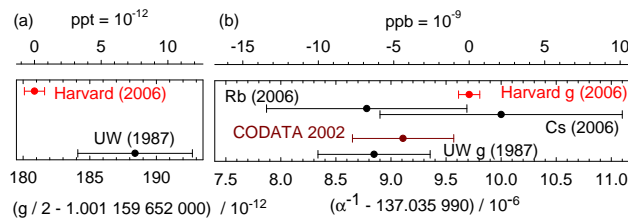


FIGURE 1. Six-fold improved electron g is 1.7 standard deviations from the last measurement (a). New α is ten times less uncertain than values of α deduced from Rb and Cs [12, 13], and the current CODATA value [7] (b). Measured g are converted to α with current QED theory.

What can be learned from a more accurate electron g ? The first result beyond g itself is a shifted and much less uncertain value for the fine structure constant, $\alpha = e^2/(4\pi\epsilon_0\hbar c)$ [2] – about ten times more accurate than nearest rival methods. This is the first uncertainty reduction since 1987 in this measure of the strength of the electromagnetic interaction, a crucial ingredient in our system of fundamental constants [7]. Second, the most stringent test of QED theory is provided, limited by ten times larger uncertainties in independent measurements of α . Third, even though muon g values have nearly 1000 times larger uncertainties [14], the muon and electron g values together are a sensitive probe for physics beyond the standard model. Calculations of the muon g depends more sensitively upon heavy particles, as well as upon α , which the electron g provides.

3. BIG IMPROVEMENT REQUIRES NEW METHODS

One electron suspended in a Penning trap is used for the new measurement, like in past. However, methods developed for the new measurement over 20 years (and reported in 6.5 Ph.D. theses) make it possible to realize an electron that resides entirely in the quantum ground state of its cyclotron motion. This “quantum cyclotron” leaves its ground state only when we deliberately send a resonant photon to excite it. The homemade “atom” that we make for the measurement is now essentially quantum mechanical rather than classical.

1. Only the lowest quantum levels of the spin and cyclotron motion are used for the measurement. The cyclotron frequency, as well as the spin frequency, is measured using quantum jump spectroscopy.

2. A Penning trap that is also a microwave cavity is used to control the radiation field. It can suppress spontaneous emission from the cyclotron motion by more than a factor of 100, giving us the averaging time that we need to resolve one quantum transitions.
3. The microwave cavity is an understandable, right circular cylinder, which makes it possible to identify the its electromagnetic modes when these are measured in situ with a method developed for this. This allows us understand, measure and control cavity shifts for the first time.
4. The trap cavity is at 0.1 mK (rather than 4.2 K in the past). This eliminates blackbody photons that would frequency excite the cyclotron ground state.
5. Great signal-to-noise for one-quantum transitions is obtained using electronic feedback to realize the first one-particle self-excited oscillator.

The new methods are powerful enough that we now aspire to a million-times-improved measurement of the antiproton magnetic moment – a moment that is about 500 times smaller than that of the electron.

The g value determines the spin frequency $\nu_s = \frac{g}{2} \nu_c$ for a free electron in a magnetic field $B\hat{z}$. To weakly confine the electron, an electric quadrupole potential, $V \sim 2z^2 - \rho^2$, is added, with $\rho = x\hat{x} + y\hat{y}$. Optimal biasing of the the electrodes (Fig. 2a) of an orthogonalized cylindrical Penning trap [11] minimizes an undesired z^4 term. The electron-trap system has four eigenfrequencies. The spin and trap-modified cyclotron frequencies are approximately equal at $\nu_s \approx \bar{\nu}_c \approx 149$ GHz. A harmonic axial oscillation along \mathbf{B} is at $\bar{\nu}_z \approx 200$ MHz, and an orthogonal circular magnetron oscillation is at $\bar{\nu}_m \approx 134$ kHz. The latter three frequencies are shifted by the unavoidable leading imperfections of a real Penning trap – harmonic distortions of the quadrupole potential, and a misalignment of the the electrode axis and \mathbf{B} [15].

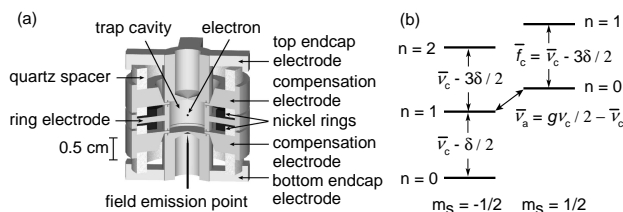


FIGURE 2. Cylindrical Penning trap cavity used to confine a single electron and inhibit spontaneous emission (a), and the cyclotron and spin levels of an electron confined within it (b).

The spin motion is undamped, being essentially uncoupled from its environment [16]. The cyclotron motion would damp in ~ 0.1 s via synchrotron radiation in free space. This spontaneous emission is greatly inhibited in the trap cavity (to 6.7 s or 1.4 s here) when \mathbf{B} is tuned so $\bar{\nu}_c$ is far from resonance with cavity radiation modes [9, 16]. Blackbody photons that would excite the cyclotron ground state are eliminated by cooling the trap and vacuum enclosure below 100 mK with a dilution refrigerator [8]. (Thermal radiation through the microwave inlet makes < 1 excitation/hr.) The axial motion, damped by a resonant circuit, cools below 0.3 K (from 5 K) when the axial detection amplifier is off for crucial periods. The magnetron motion radius is minimized with axial sideband cooling [16].

For the first time, g is deduced from observed transitions between only the lowest of the spin ($m_s = \pm 1/2$) and cyclotron ($n = 0, 1, 2, \dots$) energy levels (Fig. 2b),

$$E(n, m_s) = \frac{g}{2} h \nu_c m_s + (n + \frac{1}{2}) h \bar{\nu}_c - \frac{1}{2} h \delta (n + \frac{1}{2} + m_s)^2. \quad (2)$$

The needed $\nu_c = eB/(2\pi m)$ (for a free electron in a magnetic field) is related to the observable eigenfrequencies by the Brown-Gabrielse invariance theorem [15],

$$(\nu_c)^2 = (\bar{\nu}_c)^2 + (\bar{\nu}_z)^2 + (\bar{\nu}_m)^2, \quad (3)$$

which applies despite the mentioned imperfection shifts of the three eigenfrequencies. The third term in Eq. 2, the leading relativistic correction [16] with $\delta/\nu_c \equiv h\nu_c/(mc^2) \approx 10^{-9}$, would add uncertainty to the measurement if cyclotron energy levels were not resolved.

The anomaly and spin-up cyclotron frequencies ($\bar{\nu}_a \approx 173$ MHz and \bar{f}_c in Fig. 2b) are measured, since

$$\frac{g}{2} = \frac{\bar{\nu}_c + \bar{\nu}_a}{\nu_c} \simeq 1 + \frac{\bar{\nu}_a - \bar{\nu}_z^2/(2\bar{f}_c)}{\bar{f}_c + 3\delta/2 + \bar{\nu}_z^2/(2\bar{f}_c)}. \quad (4)$$

We use the approximation to the right which requires no measurement of $\bar{\nu}_m$. It incorporates an expansion of the invariance theorem [15], using $\bar{\nu}_c \gg \bar{\nu}_z \gg \bar{\nu}_m \gg \delta$. Corrections go as the product of $(\bar{\nu}_z/\bar{\nu}_c)^4 \sim 10^{-12}$ and a misalignment/harmonic distortion factor $\sim 10^{-4}$ [15].

A change in cyclotron or spin state is revealed by $\bar{\nu}_z$ shifts (Fig. 3a-b) of a one-electron self-excited oscillator (SEO) [10]. The electron's axial oscillation induces a signal in a resonant circuit that is amplified and fed back to drive the oscillation. QND couplings of spin and cyclotron energies to $\bar{\nu}_z$ [8] arise because saturated nickel rings (Fig 2a) produce a small magnetic bottle, $\Delta B = \beta_2[(z^2 - \rho^2/2)\hat{\mathbf{z}} - z\rho\hat{\boldsymbol{\rho}}]$ with $\beta_2 = 1540$ T/m².

Anomaly transitions are induced by applying potentials oscillating at $\bar{\nu}_a$ to electrodes, to drive an off-resonance axial motion through the bottle's $z\rho$ gradient. The electron sees the oscillating magnetic field perpendicular to \mathbf{B} as needed to flip its spin, with a gradient that allows a simultaneous cyclotron transition. Cyclotron transitions are induced by microwaves with a transverse electric field that are injected into and filtered by the cavity. The electron samples the same magnetic gradient while $\bar{\nu}_a$ and \bar{f}_c transitions are driven, because both drives are kept on, with one detuned slightly so that only the other makes transitions.

A measurement starts with the SEO turned on to verify that the electron is in the upper of the two stable ground states, $|n = 0, m_s = 1/2\rangle$. Simultaneous $\bar{\nu}_c - \delta/2$ and $\bar{\nu}_a$ drives prepare this state as needed. The magnetron radius is reduced with 1.5 s of strong sideband cooling [16] at $\bar{\nu}_z + \bar{\nu}_m$, and the detection amplifier is turned off. After 1 s, either a \bar{f}_c drive, or a $\bar{\nu}_a$ drive, is on for 2 s. The detection amplifier and the SEO are then switched on to check for a cyclotron excitation, or a spin flip (from an anomaly transition followed by a cyclotron decay). Inhibited spontaneous emission gives the time needed to observe a cyclotron excitation before an excited state decays. We step through each $\bar{\nu}_c$ and $\bar{\nu}_a$ drive frequency in turn, recording the number of quantum jumps per drive attempt. This cycle is repeated typically 30 times per night, when electrical and

magnetic noise are lower. A low drive strength keeps the transition probability below 20% to avoid saturation effects.

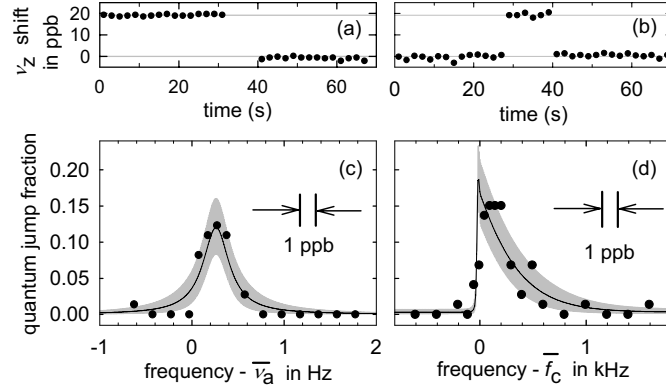


FIGURE 3. Sample \bar{v}_z shifts for a spin flip (a) and for a one-quantum cyclotron excitation (b). Quantum jump spectroscopy lineshapes for anomaly (c) and cyclotron (d) transitions, with a maximum likelihood fit to the calculated lineshapes (solid). The bands indicate 68% confidence limits for distributions of measurements about the fit values.

Quantum jump spectroscopy (measuring the quantum jumps per attempt to drive them as a function of drive frequency) gives resonance lineshapes for \bar{f}_c and \bar{v}_a (Fig. 3c-d). For weak drives that avoid saturation, the line shape comes from thermal axial motion within the magnetic bottle [17]. The small coherent axial oscillation at \bar{v}_a has no noticeable effect. However, otherwise undetectable ppb fluctuations in \mathbf{B} , on time scales shorter than an hour, could smear the Brownian motion lineshapes.

At the first of two magnetic fields used, $\bar{v}_c \approx 146.8$ GHz. A 1.4 s damping time allows good lineshape statistics (e.g., Fig. 3c-d). Three methods to extract \bar{v}_a and \bar{f}_c from lineshapes give the same g within 0.6 ppt – our “lineshape model” uncertainty in Table 1. The first method is maximum likelihood fitting of the Brownian motion lineshape. The second method fits a convolution of this lineshape and a Gaussian resolution function, about 1 ppb wide. The third method weights each drive frequency by the number of quantum jumps it produces, and uses the weighted average frequencies in Eq. 4 for \bar{v}_a and \bar{f}_c . (Well understood shifts proportional to axial temperature, common to both frequencies, do not increase the uncertainty.) This weighted average method should account for Brownian axial motion and additional fluctuations of \mathbf{B} . At our second field, where $\bar{v}_c \approx 149.0$ GHz, the 6.7 s damping time requires a long wait to make certain that a spin flip has not occurred, limiting the lineshape statistics. In this case, we use the weighted average method.

The \bar{v}_z in Eq. 4 pertains while \bar{f}_c and \bar{v}_a are driven – not what is measured when the SEO amplifier is on and increasing the axial temperature from 0.3 to 5 K. Limits on axial heating shifts come from the width of a notch in the noise spectrum resonance for the resonant circuit [16] (Table 1), measured less well for $\bar{v}_c \approx 146.8$ GHz.

Although the g -value from Eq. 4 is independent of \mathbf{B} , field stability is still an important challenge, since \bar{v}_a and \bar{f}_c are measured at different times. After the superconducting solenoid settles for several months, field drifts below 10^{-9} /night have been observed. This requires regulating five He and N₂ pressures in the solenoid and experi-

TABLE 1. Applied corrections and uncertainties for g in ppt.

Source	$\bar{\nu}_c =$	146.8 GHz	149.0 GHz
$\bar{\nu}_z$ shift		0.2(0.3)	0.00(0.02)
Anomaly power		0.0(0.4)	0.00(0.14)
Cyclotron power		0.0(0.3)	0.00(0.12)
Cavity shift		12.8(5.1)	0.06(0.39)
Lineshape model		0.0 (0.6)	0.00 (0.60)
Statistics		0.0 (0.2)	0.00 (0.17)
Total (in ppt)		13.0(5.2)	0.06(0.76)

ment cryostats, and the surrounding air temperature to 0.3 K. We correct for drifts up to 10^{-9} /hr using a cyclotron resonance edge measured once in three hours.

The trap cavity modifies the density of states of radiation modes of free space, though not enough to significantly affect QED calculations of g [18]. However, cavity radiation modes do shift \bar{f}_c [19] – still a significant uncertainty, as in the past [19, 6]. We use a trapped electron method [20] to observe the resonant radiation modes (Fig. 4a), which can be quantitatively understood in a good cylindrical Penning trap cavity [11]. Our best measurement comes from choosing $\bar{\nu}_c \approx 149.0$ GHz, maximally detuned from modes that couple to the cyclotron motion of a centered electron. A measurement at $\bar{\nu}_c \approx 146.8$ GHz, uncomfortably close to TE_{127} , checks how well cavity shifts are managed. Until the cavity spectrum and its frequency calibration is more carefully studied, TE_{127} and TM_{143} are assumed only to lie within the shaded bands. A renormalized calculation (Eq. 8.19 of [16]) gives a range of possible cavity shifts of the measured g (Fig. 4b) that is insensitive to mode quality factors for $Q > 500$. Assigned shifts and uncertainties are indicated in Fig. 4b and in Table 1. The first direct observation of a cavity shift of g , the difference between our two measurements (Fig. 4c), lies within the predicted range.

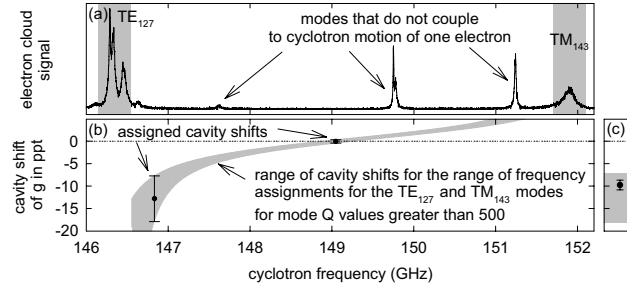


FIGURE 4. Modes of the trap cavity observed with synchronized electrons (a). Resulting assigned cavity shifts (points and Table 1) (b). First measured cavity shift of g (point) is the shift between measurements at 146.8 and 149.0 GHz (c). Gray bands are the assumed calibration and identification uncertainties for mode frequencies in (a), and the resulting range of predicted cavity shifts in (b) and (c).

A new value for the electron magnetic moment,

$$g/2 = 1.001\,159\,652\,180\,85\,(76) \quad (0.76 \text{ ppt}), \quad (5)$$

comes from the measurement at $\bar{\nu}_c \approx 149.0$ GHz. The standard deviation, about six times smaller than from any previous measurement, arises mostly from the lineshape model and cavity shifts (Table 1). Varying the $\bar{\nu}_a$ and \bar{f}_c drive power causes no detectable shifts of g .

4. DETERMINATION OF THE FINE STRUCTURE CONSTANT

The new electron g , together with QED theory, determine the fine structure constant, α , about ten times more accurately than does any rival method. QED provides an asymptotic series relating g and α ,

$$\begin{aligned} \frac{g}{2} = 1 &+ C_2 \left(\frac{\alpha}{\pi}\right) + C_4 \left(\frac{\alpha}{\pi}\right)^2 + C_6 \left(\frac{\alpha}{\pi}\right)^3 + C_8 \left(\frac{\alpha}{\pi}\right)^4 \\ &+ \dots + a_{\mu\tau} + a_{\text{hadronic}} + a_{\text{weak}}, \end{aligned} \quad (6)$$

with hadronic and weak contributions added, and assuming no electron substructure. Impressive calculations, summarized in [2], give exact C_2 , C_4 and C_6 , a numerical value and uncertainty for C_8 , and a small $a_{\mu\tau}$.

Our new value for α [2] comes from the measured g and Eq. 6,

$$\begin{aligned} \alpha^{-1} &= 137.035999710(90)(33) [0.66 \text{ ppb}] [0.24 \text{ ppb}], \\ &= 137.035999710(96) [0.70 \text{ ppb}], \end{aligned} \quad (7)$$

The first line gives the experimental uncertainty first and the QED uncertainty second, including an estimated contribution from a yet uncalculated C_{10} [2]. The total 0.70 ppb uncertainty is ten times smaller than for the next most precise methods (Fig. 1b) – determining α from measured mass ratios, optical frequencies, together with either Rb [12] or Cs [13] recoil velocities.

5. TESTING QED, AND PROBING ELECTRON STRUCTURE

The most stringent test of QED (one of the most demanding comparisons of any calculation and experiment) comes from comparing the measured and calculated $g/2$. The new g , together with $\alpha(\text{Cs})$ or $\alpha(\text{Rb})$ in Eq. 6, give a difference $|\delta g/2| < 15 \times 10^{-12}$. The small uncertainties in $g/2$ will allow a ten times more stringent test if ever the large uncertainties in the independent α values can be reduced. The prototype of modern physics theories is thus tested far more stringently than its inventors could ever have envisioned, with more to come. (See quote from Dyson letter to G.G. in Kleppner's introductory lecture for this ICAP.)

The same comparison of theory and experiment probes the internal structure of the electron [3] – limiting the electron to constituents with a mass $m^* \geq m/\delta g/2 = 34,000 \text{ TeV}/c^2$, with an electron radius $R < 6 \times 10^{-24} \text{ m}$. If this test was limited only by our experimental uncertainty in g , then we could set a limit $m^* > 600 \text{ GeV}$. These high energy limits seem somewhat remarkable for an experiment carried out at 100 mK.

6. FUTURE AND CONCLUSION

Are experimental improvements possible? A reduction of the 0.76 ppt uncertainty of the measured electron g seems likely, given that this fully quantum measurement has only recently been realized. With time to study the lineshapes and cavity shifts at many values of the magnetic field, to improve cooling methods, and to incorporate a more stable magnetic field, an improved α from g and QED seems quite possible.

In conclusion, greatly improved measurements of the electron magnetic moment and the fine structure constant, and a sensitive probe for internal electron structure, come from resolving the lowest cyclotron and spin levels of a one-electron quantum cyclotron. A self-excited oscillation of the electron reveals one-quantum transitions. A cylindrical Penning trap cavity narrows resonance lines by inhibiting spontaneous emission. Electromagnetic modes of this understandable cavity geometry, probed with synchronized electrons, shift g in a measurable way. The new $g/2$ is shifted from a long accepted value by 1.7 standard deviations, and its fractional accuracy of 7.6×10^{-13} is nearly six times smaller. The new α has an uncertainty ten times smaller than that from any other determination.

The theses of B. D'Urso [21] and B. Odom [22] give many measurement details, and a preliminary analysis is in the latter. S. Peil, D. Enzer, and K. Abdullah contributed to earlier versions of the apparatus. The NSF AMO program provided long-term funding.

REFERENCES

1. B. Odom, D. Hanneke, B. D'Urso, and G. Gabrielse, *Phys. Rev. Lett.* **97**, 030801 (2006).
2. G. Gabrielse, D. Hanneke, T. Kinoshita, M. Nio, and B. Odom, *Phys. Rev. Lett.* **97**, 030802 (2006).
3. S. J. Brodsky, and S. D. Drell, *Phys. Rev. D* **22**, 2236 – 2243 (1980).
4. A. Rich, and J. C. Wesley, *Rev. Mod. Phys.* **44**, 250 (1972).
5. R. S. Van Dyck Jr., P. B. Schwinberg, and H. G. Dehmelt, *The Electron*, Kluwer Academic Publishers, Netherlands, 1991.
6. R. S. Van Dyck, Jr., P. B. Schwinberg, and H. G. Dehmelt, *Phys. Rev. Lett.* **59**, 26–29 (1987).
7. P. J. Mohr, and B. N. Taylor, *Rev. Mod. Phys.* **72**, 377 (2000), *Rev. Mod. Phys.* **77**, 18 (2005).
8. S. Peil, and G. Gabrielse, *Phys. Rev. Lett.* **83**, 1287–1290 (1999).
9. G. Gabrielse, and H. Dehmelt, *Phys. Rev. Lett.* **55**, 67–70 (1985).
10. B. D'Urso, R. Van Handel, B. Odom, D. Hanneke, and G. Gabrielse, *Phys. Rev. Lett.* **94**, 113002 (2005).
11. G. Gabrielse, and F. C. MacKintosh, *Intl. J. of Mass Spec. and Ion Proc.* **57**, 1–17 (1984).
12. P. Cladé, E. de Mirandes, M. Cadoret, S. Guellati-Khélifa, C. Schwob, F. Nez, L. Julien, and F. Biraben, *Phys. Rev. Lett.* **96**, 033001 (2006).
13. V. Gerginov, K. Calkins, C. E. Tanner, J. McFerran, S. Diddams, A. Bartels, and L. Hollberg, *Phys. Rev. A* **73**, 032504 (2006).
14. G. W. Bennett, *et al.*, *Phys. Rev. Lett.* **92**, 161802 (2004).
15. L. S. Brown, and G. Gabrielse, *Phys. Rev. A* **25**, 2423–2425 (1982).
16. L. S. Brown, and G. Gabrielse, *Rev. Mod. Phys.* **58**, 233–311 (1986).
17. L. S. Brown, *Ann. Phys. (N.Y.)* **159**, 62–98 (1985).
18. D. G. Boulware, L. S. Brown, and T. Lee, *Phys. Rev. D* **32**, 729–735 (1985).
19. L. S. Brown, G. Gabrielse, K. Helmerson, and J. Tan, *Phys. Rev. Lett.* **55**, 44–47 (1985).
20. J. Tan, and G. Gabrielse, *Phys. Rev. Lett.* **67**, 3090–3093 (1991).
21. B. D'Urso, Ph.D. thesis, Harvard Univ. (2003).
22. B. Odom, Ph.D. thesis, Harvard Univ. (2004).